



OPEN ACCESS

EDITED BY

Alessandra Cuomo,
University of Naples Federico II, Italy

REVIEWED BY

Giuseppina Pennesi,
AST Fermo Marche Region Health System, Italy
Alice Marino,
Université Catholique de Louvain, Belgium

*CORRESPONDENCE

Melanie Ricke-Hoch,
✉ Hoch.melanie@mh-hannover.de

†These authors have contributed equally to this work and share first authorship

RECEIVED 28 August 2024

ACCEPTED 10 December 2024

PUBLISHED 06 January 2025

CITATION

Schoenherr C, Pietzsch S, Barca C, Müller FE, Bahr FS, Kasten M, Zeug A, Erschow S, Falk CS, Ponimaskin E, Thackeray JT, Hilfiker-Kleiner D and Ricke-Hoch M (2025) Immune-checkpoint-inhibitor therapy directed against PD-L1 is tolerated in the heart without manifestation of cardiac inflammation in a preclinical reversible melanoma mouse model. *Front. Mol. Med.* 4:1487526. doi: 10.3389/fmmed.2024.1487526

COPYRIGHT

© 2025 Schoenherr, Pietzsch, Barca, Müller, Bahr, Kasten, Zeug, Erschow, Falk, Ponimaskin, Thackeray, Hilfiker-Kleiner and Ricke-Hoch. This is an open-access article distributed under the terms of the [Creative Commons Attribution License \(CC BY\)](https://creativecommons.org/licenses/by/4.0/). The use, distribution or reproduction in other forums is permitted, provided the original author(s) and the copyright owner(s) are credited and that the original publication in this journal is cited, in accordance with accepted academic practice. No use, distribution or reproduction is permitted which does not comply with these terms.

Immune-checkpoint-inhibitor therapy directed against PD-L1 is tolerated in the heart without manifestation of cardiac inflammation in a preclinical reversible melanoma mouse model

Caroline Schoenherr^{1,2†}, Stefan Pietzsch^{1,3†}, Cristina Barca⁴, Franziska E. Müller⁵, Frauke S. Bahr⁵, Martina Kasten¹, Andre Zeug⁵, Sergej Erschow¹, Christine S. Falk⁶, Evgeni Ponimaskin⁵, James T. Thackeray⁴, Denise Hilfiker-Kleiner^{1,7} and Melanie Ricke-Hoch^{1*}

¹Department of Cardiology and Angiology, Hannover Medical School, Hannover, Germany, ²Department of Hematology, Hemostasis, Oncology and Stem Cell Transplantation, Hannover Medical School, Hannover, Germany, ³Department of Human Genetics, Hannover Medical School, Hannover, Germany, ⁴Department of Nuclear Medicine, Hannover Medical School, Hannover, Germany, ⁵Department of Cellular Neurophysiology, Hannover Medical School, Hannover, Germany, ⁶Institute of Transplant Immunology, IFB-Tx, Hannover Medical School, Hannover, Germany, ⁷Department of Cardiovascular Complications of Oncologic Therapies, Medical Faculty of the Philipps University Marburg, Marburg, Germany

Immune-checkpoint-inhibitors (ICI) target key regulators of the immune system expressed by cancer cells that mask those from recognition by the immune system. They have improved the outcome for patients with various cancer types, such as melanoma. ICI-based therapy is frequently accompanied by immune-related adverse side effects (IRAEs). The reversible melanoma cancer mouse model (B16F10 cells stably expressing a ganciclovir (GCV)-inducible suicide gene in C57BL/6N mice: B16F10-GCV) allows chemotherapy-free tumor elimination in advanced disease stage and demonstrates almost complete recovery of the mouse heart from cancer-induced atrophy, molecular impairment and heart failure. Thus, enabling the study of anti-cancer-therapy effects. Here, we analyzed potential cardiac side effects of antibody-mediated PD-L1 inhibition in the preclinical B16F10-GCV mouse model after tumor elimination and 2 weeks recovery (50 days after tumor inoculation). Anti-PD-L1 treatment was associated with improved survival as compared to isotype control (Ctrl) treated mice. Surviving anti-PD-L1 and Ctrl mice showed similar cardiac function, dimensions and the expression of cardiac stress and hypertrophy markers. Although anti-PD-L1 treatment was associated with increased troponin I type 3 cardiac (TNNI3) blood levels, cardiac mRNA expression of macrophage markers and elevated cardiac levels of secreted inflammatory factors compared to Ctrl treatment, both groups showed a comparable density of inflammatory cells in the heart (using CXCR4-ligand ⁶⁸Ga-Pentixafor in PET-CT and immunohistochemistry). Thus, anti-PD-L1 therapy improved survival in mice with advanced melanoma cancer with no major

cardiac phenotype or inflammation 50 days after tumor inoculation. Without a second hit that triggers the inflammatory response, anti-PD-L1 treatment appears to be safe for the heart in the preclinical melanoma mouse model.

KEYWORDS

immune checkpoint inhibitors, PD-L1, inflammation, cancer, cardio-oncology, cardiotoxicity

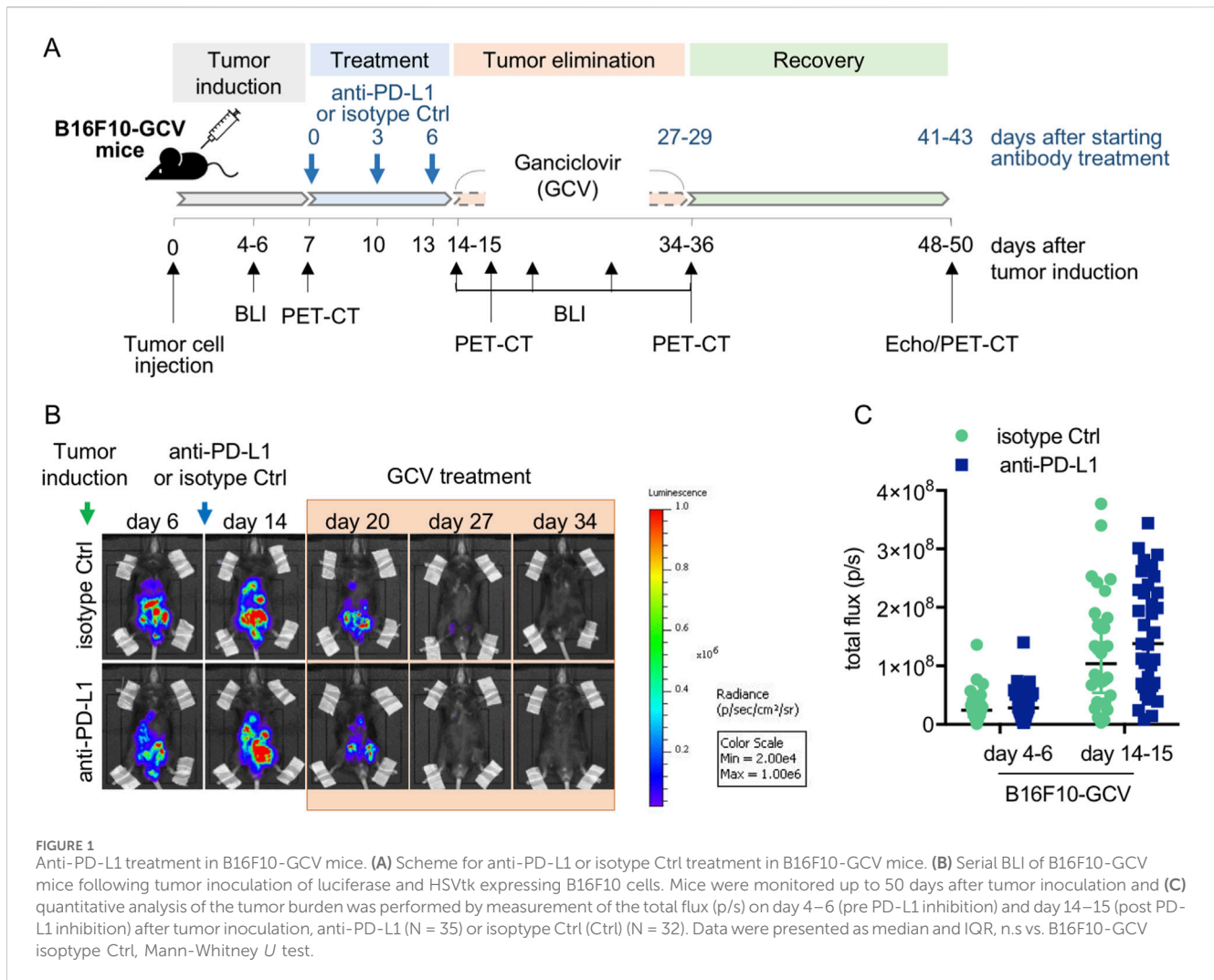
Introduction

The development and clinical use of immune checkpoint inhibitors (ICIs) have recently improved the survival of patients with various types of cancer, including malignant melanoma, lung cancer, kidney cancer and others (Palaskas et al., 2020; Mahoney et al., 2015). In contrast to conventional chemotherapy or targeted therapies that mostly have a direct effect on cancer cells, ICIs mediate their effects indirectly by enabling the immune system to recognize cancer cells mainly by tumor-specific, cytotoxic T lymphocytes. Within the group of ICIs, there exist different “generations” of drugs, each of which differ in its target molecule and thus intervene at different points of entry in the immune system, but all have in common the overarching effect of increased sensitization of the endogenous immune defense mechanisms (Varricchi et al., 2017). An immunosuppressive effect of so-called immune checkpoints is exerted by expression and mutual recognition of various cell surface markers (cytotoxic T-lymphocyte associated protein 4 (CTLA-4), programmed cell death 1 (PD-1), programmed cell death ligand 1 (PD-L1)) on T cells and antigen-presenting cells (de Mello et al., 2017). This effect protects against an “overshoot” of the immune response or autoimmune diseases during antigen recognition and subsequent T cell activation. High expression of these surface markers enables tumor cells to evade recognition and thus elimination by the immune system (de Mello et al., 2017). The blockade of this ligand receptor interaction using ICIs prevents the following immunosuppressive effect and the sensitized immune system reacts with an intensified immune response, which is now also directed against tumor cells that previously remained undetected.

An intervention in such central mechanisms of the immune response can be associated with so-called immune-related adverse events (IRAE) (Varricchi et al., 2017). Initially, the most common mild side effects observed with various ICIs were rash, fatigue, pruritus or diarrhea (Varricchi et al., 2017). Recently, increasing evidence has been reported for acute and sometimes life-threatening myocarditis related to ICI treatment (Neilan et al., 2018). Due to the acute form of ICI-associated cardiotoxicity and the demonstrated expression of PD-1/PD-L1 in the heart, this signaling pathway is assumed to be of particular importance in the development of ICI-induced myocarditis (Neilan et al., 2018). The release of heart muscle-specific proteins (cardiac antigens) due to severe cardiac atrophy, e.g., in tumor disease, could lead to sensitization to cardiac inflammation caused by ICI. FDA approved medications for PD-L1 blockade include humanized monoclonal antibodies such as Atezolizumab, Durvalumab, Avelumab (Schardt, 2020).

Previous clinical studies on cardiotoxicity frequently use healthy animal models that do not adequately capture the

clinical situation of cancer diseased patients, since cancer itself is able to impact on the cardiovascular system, such as cardiac atrophy and inflammation, alterations in mitochondrial oxidative characteristics and metabolism, and a functional decline (Pietzsch et al., 2021; Salloum et al., 2023). In addition, the systemic impact of malignant tumor diseases, including the release of cytokines and metabolites, impairs several cardioprotective signaling pathways. Therefore, the effect of anti-cancer medications on the heart may be different in healthy and in cancer diseased mice. As mouse cancer models may exhibit high mortality complicating longterm studies, we established a reversible B16F10 melanoma mouse model that was stably transduced with a suicide gene inducing cell death upon exposure to ganciclovir (GCV, model named as B16F10-GCV mice) (Pincha et al., 2011; Pietzsch et al., 2021). In B16F10-GCV mice, we have previously demonstrated almost complete cardiac recovery from cancer-induced atrophy, molecular impairment and heart failure (Pietzsch et al., 2021). In brief, during advanced cancer stage, B16F10-GCV mice showed massive cardiac atrophy related to cardiomyocyte atrophy (without the induction of cardiomyocyte apoptosis), and impaired cardiac function. Cardiac atrophy and dysfunction were partly caused by an imbalance of cardiac protein synthesis and degradation related to alterations in systemic and cardiac metabolism such as an impairment in insulin signaling (Thackeray et al., 2017; Pietzsch et al., 2021). After recovery from melanoma cancer, B16F10-GCV mice displayed functional, metabolic and morphological cardiac recovery (Pietzsch et al., 2021). Thus, this model enables investigation of longlasting effects of cancer on the cardiovascular system after chemotherapy-free tumor elimination, and to differentiate them from side effects of anti-cancer therapies (Pietzsch et al., 2021). In this context, we were already able to demonstrate that doxorubicin treatment during the advanced cancer disease stage is associated with increased mortality of B16F10-GCV mice. The surviving mice revealed morphological and functional cardiac recovery but showed longlasting alterations in the cardiac gene expression profile, especially in the circadian rhythm pathway, which is a known mediator of the DNA damage response pathway (DDR) and might contribute to late cardiotoxicity. In the present study, we applied a mouse-specific monoclonal antibody treatment regime targeting PD-L1 to investigate potential side effects of ICI therapy on the heart after recovery from tumor disease in the reversible B16F10 melanoma mouse model. Since in cancer patients with ICI therapy IRAEs often occur within a timeframe of approximately 6 weeks after ICI therapy, we performed the final analysis for our study 50 days after tumor induction and 43 days after starting anti-PD-L1 therapy. To detect possible inflammatory response during anti-PD-L1 therapy, serial ^{68}Ga -Pentixafor PET-CT measurements were done. The aim was to



analyze whether a PD-L1-directed ICI therapy induces cardiac IRAE after recovery from melanoma cancer disease. An elevated immune response after recovery from cancer disease might therefore contribute to late autoimmune side effects such as myocarditis.

Methods

B16F10 melanoma cells

Murine melanoma cell line B16F10 was obtained from ATCC. Cells were grown in DMEM culture medium containing 4.5 g/L glucose (Capricorn) supplemented with 10% FCS (Biochrom AG) and penicillin/streptomycin (100 U/100 µg per ml, Gibco). For injection, tumor cells were grown to confluence and detached from cell culture flasks by treatment with 0.25% trypsin/EDTA (Gibco). Cell pellet was washed twice with prewarmed, sterile PBS; then, cells were suspended in PBS and counted. As previously described, B16F10 cells were genetically modified by lentiviral transduction with a herpes simplex virus type 1 thymidine kinase (HSVtk), firefly luciferase and yellow fluorescent protein (YFP) containing construct (Pincha et al., 2011; Pietzsch et al., 2021). Single cell clones were isolated by limiting

dilution and checked for positive YFP signal in FACS. A fully YFP-positive cell clone (B16F10HSVtk-c) was used for all *in vivo* experiments. HSVtk1 enabling cell-specific induction of apoptosis was activated by addition of GCV as described (Tomacic et al., 2002).

Animal experiments—B16F10 melanoma mouse model

As described before, male C57BL6/N mice (12 ± 2 weeks of age, Charles River Germany) were injected intraperitoneally (i.p.) with B16F10HSVtk-c melanoma cells (B16F10 mice, 1×10^6 cells) or PBS as a vehicle (Thackeray et al., 2017; Pietzsch et al., 2021). Single doses of 100 µg monoclonal antibody per animal against PD-L1 (GolnVivo™ purified anti-mouse CD274 antibody clone 10F.9G2, no 124328, BioLegend) or corresponding isotype control (Ctrl, GolnVivo purified rat IgG2b,k isotype Ctrl, no 400666, BioLegend) were applied i.p. at day 7, 10, and 13 after tumor cell or PBS injection for a total of 3 doses (Figure 1A, Supplementary Figure S1A). Treatment with GCV (80 mg/kg BW twice daily) was started at advanced tumor disease stage at day 14 based on the guidelines of recognition of distress in experimental animals

proposed by Morton and Griffith (Figure 1A) (Morton and Griffiths, 1985). Using the same protocol, GCV treatment of cancer-free control mice (GCV mice) was started at day 14 after PBS vehicle injection (Supplementary Figure S1A). GCV treatment was continued until day 34–36 when signal loss in IVIS B16F10-GCV mice occurred. For live visualization of B16F10 melanoma cells, mice were imaged using an *in vivo* imaging system (IVIS) Lumina II (Caliper Life Sciences) for 1 min following i.p. injection of 0.8 mg/mouse D-Luciferin (AppliChem). Whole animal imaging was performed from a ventral perspective. Bioluminescence radiance was analyzed using Living Image (BLI) 4.0 software. After melanoma cell inoculation, B16F10-GCV and GCV mice received continuous analgesia (Novalgin, 500 mg/mL in drinking water). Mice were housed in groups of five and maintained on a 14 h/10 h light/dark cycle with standard laboratory chow and water freely available. Animal health condition was assessed based on the guidelines of recognition of distress in experimental animals as proposed by Morton and Griffith (Morton and Griffiths, 1985).

All animal studies were in accordance with the German animal welfare legislation and with the European Communities Council Directive 86/609/EEC and 2010/63/EU to protect animals used for experimental purposes under consideration of the ARRIVE guidelines. Furthermore, the experiments were approved by the local Institutional Animal Care and Research Advisory Committee and permitted by the local authority.

Echocardiography

Echocardiography was performed on anesthetized mice as described previously (Thackeray et al., 2017; Pietzsch et al., 2021). In brief, contractile function and heart rate were assessed by echocardiography using the Vevo 3100 system (VisualSonics) after tumor elimination and 2 weeks recovery (day 50 ± 3 after tumor cell injection). Anesthesia was induced with 4% (in 100% oxygen) isoflurane, followed by maintenance at 0.5%–1% isoflurane via a special vaporizer for rodents delivered by a small nose cone (VisualSonics). For echocardiographic image acquisition, the animal was placed in a supine position on a prewarmed platform and the body temperature was maintained at 37°C during the entire procedure. Echocardiographic measurements were obtained 5 min following the induction of anesthesia when heart rate had stably recovered to exclude the variation in cardiac function created by time after induction. Parasternal short- or long-axis views were recorded in B- and M-mode at the level of the papillary muscle, and still images were used to measure LV end-diastolic diameter (LVEDD) and LV end-systolic diameter (LVESD) and calculate fractional shortening $[(LVEDD-LVESD)/LVEDD \times 100]$. Cardiac output was calculated by VisualSonics Vevo 3100 software version 3.

Serial ⁶⁸Ga-Pentixafor PET-CT imaging protocol

As previously described, ⁶⁸Ga-Pentixafor was synthesized by using an automated module and CPCR4.2 precursor provided by

Scintomics GmbH (Fürstenfeldbruck, Germany) (Thackeray et al., 2015). ¹⁸F-FDG (fluorodeoxyglucose) was synthesized using standard kits and production methods. PET was performed using a dedicated small animal system (Inveon DPET, Siemens, Knoxville) as reported before (Thackeray et al., 2015). Animals underwent serial imaging using the CXCR4-ligand ⁶⁸Ga-Pentixafor measured in PET-CT imaging at day 7, day 15, day 35 and day 49 after tumor cell inoculation (day 0, day 8, day 28 and day 42 after starting anti-PD-L1 or isotope Ctrl treatment) to identify tissue inflammation (Figure 1A). In brief, anesthetized animals (1.5% isoflurane, 0.6 L/min O₂) were positioned prone on the imaging bed (Minerve) with the heart centered in the scanner field of view. ⁶⁸Ga-Pentixafor (12.6 ± 1.3 MBq) was injected intravenously as 0.10 mL bolus via the tail vein. After conscious tracer distribution, a 10 min static listmode scan was acquired at 50 min after injection under isoflurane anesthesia. Afterwards, 0.2 mL ¹⁸F-FDG (20 ± 2 MBq) was administered i.p. under anesthesia to enable accurate localization of the myocardium. After 20 min under continued isoflurane, a second 10 min static scan was performed (Glaserapp et al., 2021).

All PET images were reconstructed to a 128 × 128 × 159 image matrix (0.78 × 0.78 × 0.80 mm) using an OSEM3D/MAP (ordered subset expectation maximization/maximum *a posteriori*) algorithm ($\beta = 0.01$, 2 OSEM iterations, 18 MAP iterations) with scanner-applied scatter correction. A ⁵⁷Co transmission scan (10 min) was used for attenuation correction (Thackeray et al., 2015). Image analysis was performed with Inveon Research Workplace 4.2 (Siemens Medical Solutions). First, ¹⁸F-FDG images were used to manually create regions of interest for LV myocardium by interactive thresholding as previously described (Thackeray et al., 2015). These regions of interest were imported onto co-registered ⁶⁸Ga-pentixafor images to calculate ⁶⁸Ga-pentixafor uptake. The signal was semiquantitatively analyzed as percent injected dose per gram of tissue (%ID/g).

Murine plasma measurements

Murine plasma samples were acquired by 10 min centrifugation at 1,500 rpm of right ventricular blood in ethylenediaminetetraacetic acid (EDTA) containing vials and stored at –80°C. Mouse troponin I type 3 cardiac (TNNI3; Novus Biologicals #NBP3-00456) levels were measured in plasma using a commercial ELISA kit following the manufacturer's protocol. Concentrations were detected with a Thermo Scientific Varioskan Flash plate reader using SkanIt Software 2.4.5 (Thermo Scientific).

Lipid peroxidation (malondialdehyde, MDA) detection

Lipid peroxidation (nmol/mg protein) were measured in LV tissue lysates using a commercial MDA assay kit (Abcam ab118970) respectively, according to the manufacturer's protocol. Concentrations were detected with a Thermo Scientific Varioskan Flash plate reader using SkanIt Software 2.4.5 (Thermo Scientific).

Histology and immunostaining

For cardiac morphological analyses, hearts were perfused, embedded in OCT Tissue-Tek and frozen at -80°C . Cardiac cryosections were stained with H&E as described (Hilfiker-Kleiner et al., 2004). Cardiomyocyte cross-sectional area (CSA) was determined on longitudinal cardiac sections of B16F10-GCV mice after staining with Fluorescein-labelled wheat germ agglutinin (WGA; Vector Laboratories Inc., FL-1021) and Hoechst 33258 (SIGMA-Aldrich) as previously described. At least 30–50 cells per individual heart were measured (Heimerl et al., 2020). Interstitial collagen was analysed in picro-Sirius red F3BA-stained LV cryosections (Hilfiker-Kleiner et al., 2004). Global inflammation was stained in LV cryosections with the pan-inflammatory marker CD45 (BD Pharmingen, Clone 30-F11, #550539) counterstained with eosin as described (Hoch et al., 2011). The average number of CD45⁺ cells was determined per field (5 fields/section and 3 sections/animal). HE, Sirius Red and CD45 staining images were acquired by bright field microscopy using Axio Observer 7 and Zen 2.6 pro software (Carl Zeiss Jena).

Inflammation was stained in LV cryosections with antibodies recognising CD68 (abcam ab53444), CD80 (abcam ab106162), CD206 (R&D Systems AF2535) and CD8a (Cell Signaling Technologies #98941) counterstained with Hoechst 33258 (SIGMA-Aldrich). Cardiac slices were imaged on a Zeiss LSM780 with a LD C-Apochromat 40x/1.2 W objective and Zen2013 imaging software in online-fingerprinting mode with pre-defined spectra for each fluorescent protein obtained from single stainings. Five regions per slice were randomly chosen along the sagittal axis and z-stacks were acquired with 12 planes in 0.5 μm distance and a pixel size of 0.208 μm (1024×1024 pixels, pixel dwell time 1.57 μs). Image analysis was done in maximum-intensity projections using ImageJ and Matlab (Mathworks). Mean fluorescence intensities were measured using ImageJ 'Measure' tool for each individual channel in each of the five imaged regions. A mean of the five regions was taken to represent the mean fluorescence per animal.

Number of macrophages was counted manually using ImageJ "CellCounter" Plugin in a merged image of CD68, CD80 and CD206 fluorescence signal in each of the five imaged regions. Cells were only counted when the macrophage marker signal could be assigned to a Hoechst-stained nucleus. A mean of the five regions was used to display the mean number of macrophages per animal per field of view. Pearson's correlation coefficient was calculated using custom-written Matlab scripts for each of the five regions per animal. Analysis strategy follows the colocalization theory of Scientific Volume Imaging (<https://svi.nl/ColocalizationTheory>).

Negative control for the correlation coefficient was obtained for each image by rotation of the second channel by 90°C and 50% pixel shift followed by the same correlation analysis as for the original image.

Multiplex assays of cardiac murine tissue

For multiplex analysis, samples from LV tissue of anti-PD-L1 and isotype Ctrl treated mice were generated with the Bio-

Plex[®] cell lysis kit (#171304011, Bio-Rad) according to the manufacturer's protocol. The protein concentration of the LV lysates was measured with Bradford reagent (Bio-Rad) and LV lysates were diluted with Bio-Plex sample diluent to a protein concentration of 1 mg/mL. The Bio-Plex Pro[™] Mouse Cytokine 23-plex Assay (M60009RDPD, Bio-Rad) was used as recommended by the manufacturer and measured with the Bio-Plex 200 system (Bio-Rad).

RNA isolation, cDNA synthesis and qRT-PCR

Total RNA from adult murine hearts was isolated with TRIzol[®] Reagent (Life technologies) in accordance with the manufacturer's instructions. cDNA synthesis using Superscript III (Invitrogen), 2 μg of total RNA and random hexamer primers (SIGMA-Aldrich) was performed according to the manufacturer's protocols as previously described (Heimerl et al., 2020). Semi-quantitative real-time PCR using the SYBR green dye method (SYBR Green qPCR 2xMastermix-Kit, Thermo Fisher Scientific) was performed with the AriaMX Real-Time PCR System (Agilent Technologies). Sequences of qRT-PCR primers used in this study are provided below. mRNA expression levels were normalised using the $2^{-\Delta\Delta\text{CT}}$ method relative to 18S.

Protein isolation, SDS-PAGE and Western blot

Protein expression levels were determined by Western blotting, using SDS-PAGE as described (Heimerl et al., 2020). In brief, total protein was isolated by lysing frozen LV tissue in RIPA buffer supplemented with 10 μM 1,4-dithiothreitol (SIGMA-Aldrich) and protease/phosphatase inhibitor cocktail (Roche Diagnostics) on ice. For SDS-PAGE, 50 μg protein was loaded and blotted to a nitrocellulose membrane after separation. The following primary and secondary antibodies were used: ATPase Sarcoplasmic/Endoplasmic Reticulum Ca^{2+} Transporting 2 (ATP2A2/SERCA2, dilution 1:1000; Cell Signaling Technology #4388), CD80 (dilution 1:1000; Cell Signaling Technology #54521), Programmed Cell Death 1 (PD-1, dilution 1:1000; Cell Signaling Technology #84651), phospho-Phospholamban (Ser16/Thr17) (PLN, dilution 1:1000; Cell Signaling Technology #8496), PLN (dilution 1:1000; Cell Signaling Technology #14562), cardiac Troponin T (TnT, dilution 1:2000; proteintech 15513-1-AP), CD206 (dilution 1:200; R&D Systems AF2535) and donkey anti-rabbit IgG, peroxidase-linked species-specific whole antibody NA934V (dilution 1:3000; GE Healthcare). Chemiluminescence detection was carried out after incubation with enhanced chemiluminescence reagents (PerkinElmer) using the ChemiDoc[™] MP system (Bio-Rad). Image LabV5.0 software (Bio-Rad) was used for quantification.

Statistical analyses

Statistical analysis was performed using GraphPad Prism version 7.0 or 8.0 for Mac OS X (GraphPad Software, San Diego California United States). The Shapiro-Wilk test was used to test the

Sequences of qRT-PCR primers

mRNA	Sense primers (5' to 3')	Antisense primers (5' to 3')
mmu <i>18S</i>	GTAACCCGTTGAACCCATT	CCATCCAATCGGTAGTAGCG
mmu <i>Adcy5</i>	GAAGTCCAGCTTCGGAGAG	CAGCCCGAGGTGAGAAGTA
mmu <i>Adcy6</i>	TGGGGTTTGACGACACTGAG	GCAGAGCGGAAGTCTTAGA
mmu <i>Adrge1</i>	GAGACATCCACTCTGGGCAC	GGGGCCCTGTAGATACTGA
mmu <i>Anp</i>	GCCGGTAGAAGATGAGGTCA	GGGCTCCAATCTGTCAATC
mmu <i>Atp2a2</i>	CAAACCAGATGTCGGTGTGC	TGATGGCACTTCACTGGCTT
mmu <i>Bnp</i>	ATCCGATCCGGTCTATCTTG	CCAGTCTCCAGAGCAATCA
mmu <i>Cd4</i>	GCAAAGTCTCGAGCCCTCAT	GCACATGGTGGTCTCCTGA
mmu <i>Cd8a</i>	GGATTGGACTTCGCCTGTGA	TGGGACATTTGCCAAACACGC
mmu <i>Cd19</i>	TCATTGCAAGGTCAGCAGTGTG	GGGTCAGTCATTTCGCTTCCTT
mmu <i>Cd38</i>	ACTGGAGAGCCTACCACGAA	AGTGGGGCGTAGTCTTCTCT
mmu <i>Cd80</i>	TTCAGACCGGGGCACATAC	AGAAGCGAGGCTTTGGGAAA
mmu <i>Cd206</i>	GATGACCTGTGCTCGAGAGG	TCGCTTCCCTCAAAGTGCAA
mmu <i>Col1a1</i>	ACAGACGAACAACCCAAACT	GGTTTTTGGTCACGTTCACT
mmu <i>Il-1β</i>	GCCCATCTCTGTGACTCAT	AGGCCACAGGTATTTTGTCTG
mmu <i>αMHC</i>	GGAAGAGCGAGCGGCATCAAGG	GTCTGCTGGAGAGGTTATTCCTCG
mmu <i>βMHC</i>	CAAGTTCGCAAGGTGC	AAATGTGCTTTATTCTGCTTCCAC
mmu <i>MnSOD</i>	ACCTGCCTTACGACTATGGC	AGCCTGAACCTTGGACTCC
mmu <i>Pd-11</i>	GGCAGGAGAGGAGGACCTTA	TGCAGCTTGACGTCTGTGAT
mmu <i>Ryr2</i>	CATGACCAACCCTGTCCCTGTG	CTTCCGGCTCCCATAGCG
mmu <i>Tnfα</i>	GGTGCCTATGTCTCAGCCTCTT	GCCATAGAAGTATGATGAGAGGGAG

data against the hypothesis of normal distribution. Continuous parametric data were expressed as mean \pm SD, and in the case of non-parametric data, the median and interquartile range (IQR) were reported. Differences between groups were analysed by unpaired two-tailed Student's *t*-test or Mann-Whitney *U* test dependent on data distribution. A *p*-value of <0.05 was considered statistically significant.

Results

PD-L1 inhibition showed no effect on cardiac function and morphology but was associated with increased survival of B16F10-GCV mice after tumor elimination and recovery

Male C57BL6/N mice were inoculated with the B16F10HSVtk-c melanoma cell line (B16F10 mice) as previously described (Pietzsch et al., 2021). Therefore, B16F10 mice were injected i.p. with 1×10^6 cells to induce tumor growth (Figure 1A). At day 7 after tumor cell injection, mice ($N = 80$) were randomized to groups ($N = 40$) receiving anti-PD-L1 or isotype control (Ctrl) treatment. At day 14, GCV

treatment was started until complete tumor elimination on day 34–36 (named as B16F10-GCV mice; Figure 1A). After 14 days of recovery (day 48–53), mice were subjected to echocardiography or PET-CT measurement followed by organ harvesting for further analysis (Figure 1A). Tumor progression and elimination was visualized by non-invasive BLI measurements, which demonstrated that PD-L1 targeting itself had no effect on tumor burden in surviving mice (Figures 1B, C). However, B16F10-GCV mice with anti-PD-L1 treatment showed an improved survival rate compared to isotype Ctrl treated mice 50 days after tumor inoculation and 43 days after starting anti-PDL1 or isotype Ctrl treatment (Figure 2A). In surviving mice 50 days after tumor inoculation, echocardiographic analyses demonstrated comparable cardiac function and LV dimensions in anti-PD-L1- and isotype Ctrl-treated B16F10-GCV mice (Table 1). In addition, LV tissue morphology, collagen content (as determined by Sirius Red staining), cardiac weights and cardiomyocyte cross-sectional area (CSA) revealed no alterations between both groups (Table 1, Figures 2B–D, G–I). Moreover, the cardiac mRNA expression of the hypertrophy and heart failure markers *Anp* and *Bnp* and the fibrosis marker *Col1a1* were not affected by PD-L1 inhibition (Figures 2D–F). Age-matched GCV control mice without cancer (GCV mice) were treated according to the same protocol with anti-PD-L1 or

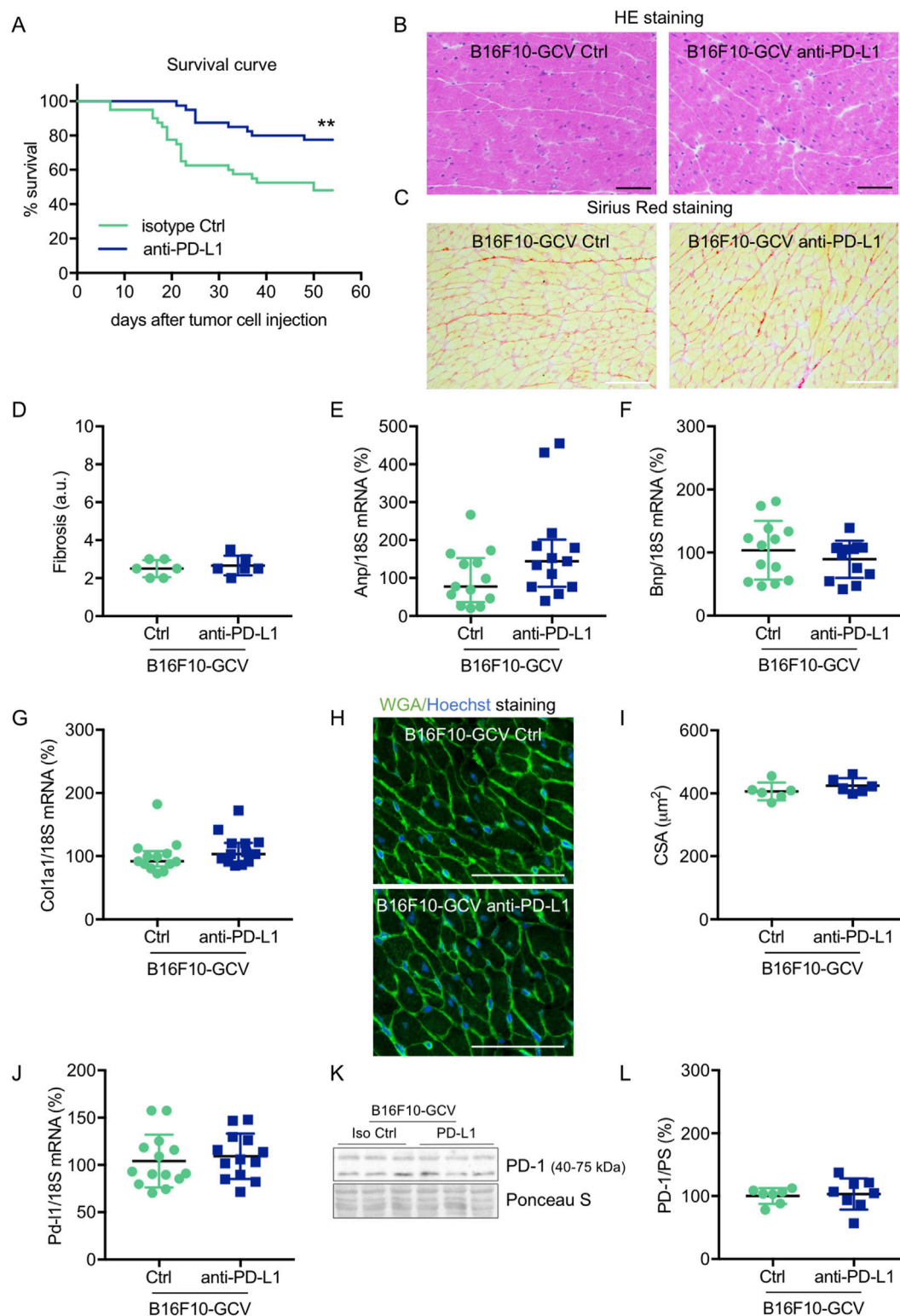


FIGURE 2

Cardiac phenotype of anti-PD-L1 treatment in B16F10-GCV mice after tumor elimination and recovery. **(A)** Kaplan-Meier survival curve for B16F10-GCV mice treated with anti-PD-L1 (N = 40) or isotype Ctrl (Ctrl) (N = 40). Log-rank test was used for statistical survival analysis, ** $p < 0.01$. **(B)** Representative sections with hematoxylin and eosin (HE) staining visualising cardiac morphology of LV cryosections from anti-PD-L1 or isotype Ctrl treated B16F10-GCV mice after tumor elimination and recovery; scale bars indicate 50 μm . **(C)** Representative images of Sirius red staining visualizing fibrosis and collagen deposits in LV cryosections from anti-PD-L1 or isotype Ctrl treated B16F10-GCV mice after tumor elimination and recovery; scale bars indicate 50 μm . **(D)** Quantification of fibrosis from anti-PD-L1 (N = 6) or isotype Ctrl (N = 6) treated B16F10-GCV LVs after tumor elimination and recovery in arbitrary units (a.u.). Dot plots summarizing **(E)** *Anp*, **(F)** *Bnp* and **(G)** *Col1a1* mRNA levels normalized to 18S RNA analysed by qRT-PCR in B16F10-GCV LVs treated with anti-PD-L1 (N = 13) or isotype Ctrl (N = 13). **(H)** Representative images of Fluorescein-labelled wheat germ (Continued)

FIGURE 2 (Continued)

agglutinin (WGA, green) and Hoechst 33528 (blue) staining of LV cryosections from anti-PD-L1 or isotype Ctrl treated B16F10-GCV mice after tumor elimination and recovery; scale bars indicate 50 μ m. **(I)** Quantification of CSA from anti-PD-L1 (N = 6) or isotype Ctrl (N = 6) treated B16F10-GCV LVs after tumor elimination and recovery. **(J)** Dot plot summarizing *Pd-I1* mRNA levels normalized to 18S RNA analysed by qRT-PCR in B16F10-GCV LVs treated with anti-PD-L1 (N = 14) or isotype Ctrl (N = 13). **(K)** Representative cardiac PD-1 western blot and **(L)** dot plot summarizing quantification of cardiac PD-1 protein expression normalised to Ponceau S staining in cardiac tissue of B16F10-GCV LVs treated with anti-PD-L1 (N = 8) or isotype Ctrl (N = 7). Uncropped full length images are presented in SFig. 5A + B. **(D, F, G, I, J, L)** Gaussian distributed data were presented as mean \pm SD and **(E)** not normally distributed data were presented as median and IQR, ***p* < 0.01 vs. B16F10-GCV isotype Ctrl, unpaired two-tailed Student's t-test or Mann-Whitney *U* test.

TABLE 1 Cardiac function and dimensions, body weight and tibia length in B16F10-GCV and GCV mice treated anti-PD-L1 or isotype Ctrl after tumor elimination and recovery.

Parameters	GCV Isotype Ctrl (N = 12)	GCV Anti-PD-L1 (N = 9)	B16F10-GCV Isotype Ctrl (N = 9)	B16F10-GCV Anti-PD-L1 (N = 13)
FS (%)	35.1 \pm 4.2	36.7 \pm 3.7	32.2 \pm 4.8	33.6 \pm 5.7
LVEDD (mm)	4.2 \pm 0.2	4.2 \pm 0.2	4.3 \pm 0.3	4.2 \pm 0.3
LVESD (mm)	2.7 \pm 0.2	2.7 \pm 0.3	2.9 \pm 0.3	2.8 \pm 0.3
Heart rate (bpm), median (IQR)	606 (576–620)	595 (580–610)	602 (591–624)	590 (544–609)
Cardiac output (mL/min), median (IQR)	20.1 (17.3–21.2)	19.8 (18.5–22.2)	19.9 (17.2–21.6)	18.3 (17.2–20.6)
HW (mg)	110.5 \pm 8.0	110.1 \pm 5.9	108.8 \pm 13.9	105.4 \pm 11.3
BW (g)	26.8 \pm 1.7	27.0 \pm 1.6	26.3 \pm 1.3	24.8 \pm 2.1*
HW/BW ratio, median (IQR)	4.1 (4.1–4.2)	4.1 (3.9–4.2)	4.1 (3.9–4.2)	4.2 (4.2–4.4)
Tibia length (TL, mm), median (IQR)	16.8 (16.8–16.9)	16.8 (16.7–16.9)	16.8 (16.7–16.9)	16.8 (16.8–16.8)
HW/TL ratio, median (IQR)	6.5 (6.1–7.0)	6.6 (6.3–6.8)	6.4 (5.9–6.8)	6.1 (6.0–7.1)

Fractional shortening (FS), left ventricular end-diastolic diameter (LVEDD), left ventricular end-systolic diameter (LVESD), heart rate (beats per minute, bpm) determined in B-mode; cardiac output determined in M-mode from echocardiographic analyses and heart weight (HW), body weight (BW), HW/BW ratio, tibia length (TL) and HW/TL ratio determined in B16F10-GCV and GCV mice treated with anti-PD-L1 or isotype Ctrl (Ctrl) after tumor elimination and recovery. Data are shown as mean \pm SD, or median (IQR), **p* < 0.05 vs. GCV anti-PD-L1, using unpaired two-tailed Student's t-test.

isotype Ctrl and showed the same cardiac function, dimensions, cardiac and body weights and gene expression as B16F10-GCV mice after tumor elimination and recovery (Supplementary Figures S1A–D, Table 1). Cardiac *Pd-I1* mRNA and PD-1 protein expression was not altered after tumor elimination and recovery in B16F10-GCV mice (Figures 2J–L; Supplementary Figures S5A, B).

Anti-PD-L1 treatment increased circulating TNNI3 levels and induced cardiac expression of α MHC and TnT after tumor elimination and recovery

To investigate whether anti-PD-L1 treatment during tumor disease is inducing cardiac damage and remodeling processes after tumor elimination and recovery, cardiac transcripts and proteins in the LV and circulating plasma proteins of B16F10-GCV and GCV mice were measured. Indeed, anti-PD-L1 treatment in B16F10-GCV mice was associated with a significant increase in cardiac α MHC mRNA and TnT protein expression, and elevated plasma troponin I type 3 (cardiac, TNNI3) levels compared to isotype Ctrl treated

B16F10-GCV mice, while β MHC mRNA expression or the ratio of β MHC/ α MHC was not affected (Figures 3A–F; Supplementary Figures S6A, B). In addition, the cardiac mRNA expression of several myocardial genes involved in the contractile/calcium handling machinery including ryanodine receptor 2 (*Ryr2*) and adenylate cyclase (*Adcy*) 5 and 6 was increased in anti-PD-L1-treated compared to isotype Ctrl-treated B16F10-GCV mice, while *ATPase sarcoplasmic/endoplasmic reticulum Ca²⁺ transporting 2* (*Atp2a2*, also known as *Serca2*) mRNA expression was not affected. (Figures 3G–J). Moreover, cardiac ATP2A2 and phospholamban (PLN) protein expression or activation was not changed in anti-PD-L1-treated B16F10-GCV mice compared to isotype Ctrl-treated B16F10-GCV mice (Figures 3K, L; Supplementary Figures S2A–D, 5B, 7A, B, 8A–C). In contrast, anti-PD-L1 treatment in GCV mice without former cancer disease showed no alterations in the expression of these cardiac transcripts or proteins except for *Ryr2* mRNA expression (Supplementary Figures 1E–M, Supplementary Figures 6C, D). The *Ryr2* mRNA expression was also increased in the anti-PD-L1-treated GCV mice compared to isotype Ctrl GCV mice suggesting that anti-PD-L1 *per se* increases cardiac expression independently of cancer disease.

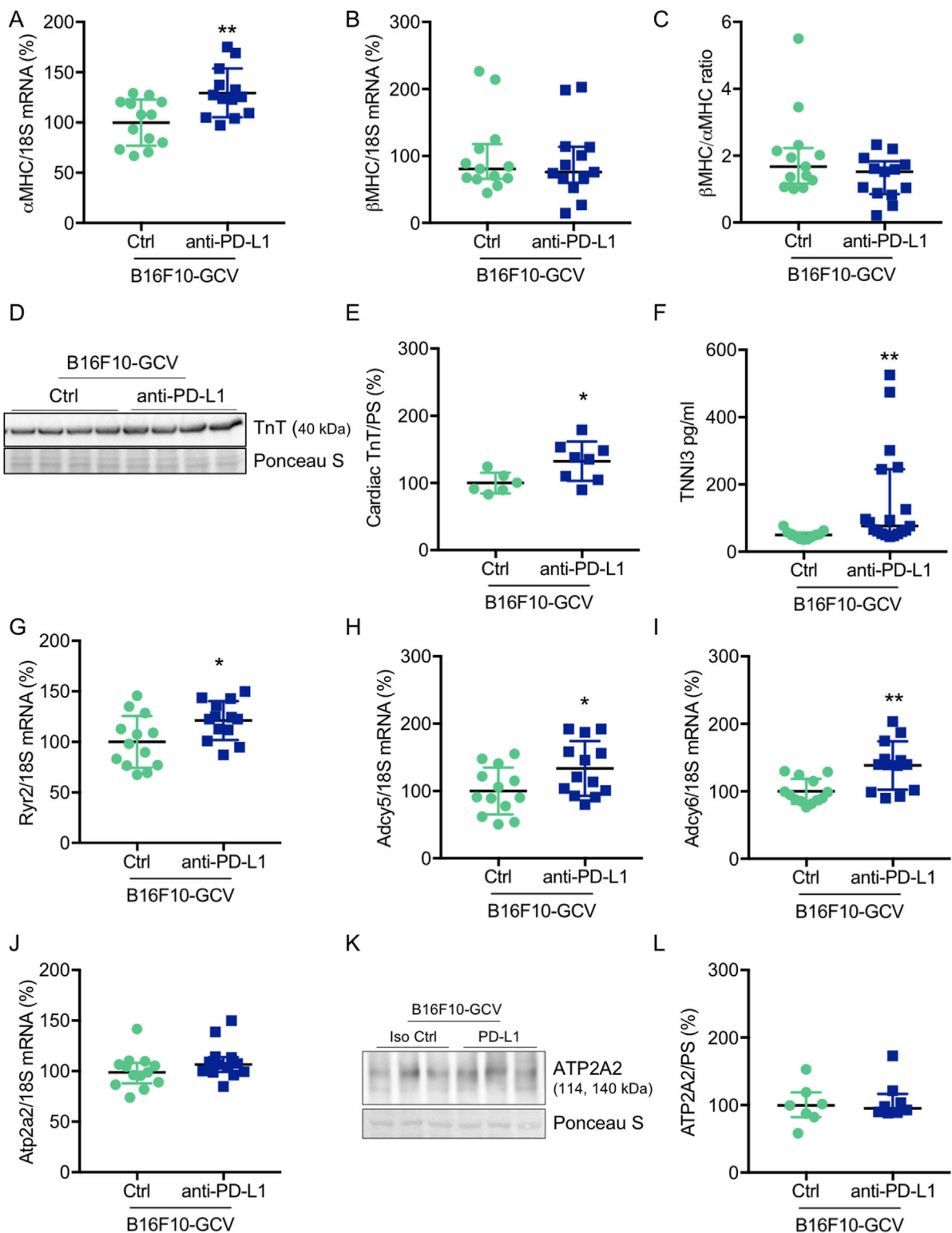


FIGURE 3

Cardiac effects of anti-PD-L1 treatment in B16F10-GCV mice. Dot plots summarizing (A) α MHC and (B) β MHC mRNA levels normalized to 18S RNA analysed by qRT-PCR in B16F10-GCV LVs treated with anti-PD-L1 (N = 13) or isotype Ctrl (N = 13). (C) Ratio of β MHC/ α MHC mRNA expression of B16F10-GCV LVs treated with anti-PD-L1 (N = 13) or isotype Ctrl (N = 13). (D) Representative cardiac TnT western blot and (E) dot plot summarizing quantification of cardiac TnT protein expression normalised to Ponceau S staining in cardiac tissue of B16F10-GCV LVs treated with anti-PD-L1 (N = 8) or isotype Ctrl (N = 6). Uncropped full length images are presented in SFig. 6A + B. (F) The dot plots summarize circulating plasma troponin I type 3 (cardiac, TNNI3) levels from B16F10-GCV mice treated with anti-PD-L1 (N = 19) or isotype Ctrl (N = 11). Dot plots summarizing (G) *Atp2a2*, (H) *Adcy5*, (I) *Adcy6* and (J) *Ryr2* mRNA levels normalized to 18S RNA analysed by qRT-PCR in B16F10-GCV LVs treated with anti-PD-L1 (N = 13) or isotype Ctrl (N = 13). (K) Representative cardiac ATP2A2 western blot and (L) dot plot summarizing quantification of cardiac ATP2A2 protein expression normalized to Ponceau S staining in

(Continued)

FIGURE 3 (Continued)

cardiac tissue of B16F10-GCV LVs treated with anti-PD-L1 (N = 8) or isotype Ctrl (N = 7). Uncropped full length images are presented in SFig. 7A + B. (A, E, H–J) Gaussian distributed data were presented as mean \pm SD and (B, C, F, G, L) not normally distributed data were presented as median and IQR, * $p < 0.05$, ** $p < 0.01$ vs. B16F10-GCV isotype Ctrl, unpaired two-tailed Student's t-test or Mann-Whitney *U* test.

In addition, to investigate putative myocardial oxidative stress, we determined the mRNA expression of *mangan superoxide dismutase* (*MnSOD*) levels and lipid peroxidation as a lipid marker for oxidative stress in LVs from B16F10-GCV mice treated with anti-PD-L1 or isotype Ctrl. No alterations were found in the cardiac *MnSOD* mRNA expression or in the detection of MDA as the end product of lipid peroxidation in B16F10-GCV LVs treated with anti-PD-L1 or isotype Ctrl (Supplementary Figures 2E, F).

Anti-PD-L1 treatment increased cardiac mRNA expression of macrophage inflammatory markers and induced the production and secretion of cardiac cytokines and chemokines

To investigate the effect of anti-PD-L1 treatment on inflammatory cyto- and chemokine production after melanoma cancer disease, a multiplex assay was performed to compare the concentration of 23 different inflammatory cytokines and chemokines in LV tissue of anti-PD-L1 and isotype Ctrl treated B16F10-GCV mice after tumor elimination and recovery (50 days after tumor induction and 43 days after starting anti-PD-L1 or isotype Ctrl treatment). Indeed, PD-L1 inhibition was associated with a significant induction of 11 cytokines/chemokines including interleukin (IL) 9, IL-12 (p40), IL-13, Eotaxin, granulocyte-colony stimulating factor (G-CSF), granulocyte-macrophage colony stimulating factor (GM-CSF), interferon γ (IFN γ), regulated on activation in normal T-Cell expressed and secreted (RANTES) and tumor necrosis factor α (TNF α) in LVs of B16F10-GCV mice (Figure 4A, Supplementary Figures 3A–V). In addition, mRNA expression of the macrophage markers *Cd206*, *Cd80* and *Cd38*, and the inflammatory marker *Il-1 β* was increased in the LV of anti-PD-L1-treated compared to isotype Ctrl-treated B16F10-GCV mice (Figures 4B–J), while mRNA levels of the B cell marker *Cd19* and the T cell markers *Cd4* and *Cd8a* were not affected. Anti-PD-L1 treatment in GCV mice without former cancer disease revealed no alterations in the cardiac expression of inflammatory or macrophage markers, suggesting that the induction of the inflammatory response observed in B16F10-GCV mice treated with anti-PDL-1 is cancer dependent (Supplementary Figures S4A–I).

Anti-PD-L1 treatment did not increase cardiac inflammation in B16F10-GCV mice after tumor elimination and recovery

To determine whether the observed increase in cardiac mRNA expression of inflammatory macrophage markers and cytokine/chemokine secretion in anti-PD-L1-treated B16F10-

GCV mice is associated with an elevated number of inflammatory cells in the heart, the inflammatory phenotype/status was determined by serial PET-CT measurements for the CXCR4-ligand ^{68}Ga -Pentixafor and fluorescence microscopy for T cell lymphocytes and macrophage makers (Figure 1A, Figures 5–7). PET-CT measurements of the CXCR4 ligand ^{68}Ga -Pentixafor in B16F10-GCV mice were performed at the indicated timepoints (Figure 1A), including before and after PD-L1 inhibition, as well as after GCV treatment and following the recovery phase. Serial PET-CT measurements identified a temporal shift in ^{68}Ga -pentixafor distribution over the progression from tumor inoculation to tumor elimination (Figures 1A, 5A). Diffuse CXCR4 signal in the LV was increased in both groups, anti-PD-L1 and isotype Ctrl treatment, after GCV-mediated tumor elimination, on day 35, but to a lesser extent in anti-PD-L1-treated animals (Figure 5B). This signal returned to baseline levels by 49 days after tumor induction. Quantitative analysis described no significant difference in the CXCR4 PET signal between PD-L1 inhibitor and isotype Ctrl after the treatment phase (day 15) or following the recovery phase (49 days after tumor induction, 42 days after starting anti-PD-L1 or isotype Ctrl treatment) (Figure 5C). By contrast, the increase of the ^{68}Ga -Pentixafor signal after GCV administration (day 35) was moderately higher in isotype Ctrl-compared to anti-PD-L1-treated mice.

Global inflammation determined by CD45 staining revealed a similar number of CD45⁺ cells in B16F10-GCV hearts treated with anti-PD-L1 or iso Ctrl at day 50 after tumor induction (43 days after starting anti-PD-L1 or isotype Ctrl treatment) (Figures 6A,B). Fluorescence immunostaining of cardiac sections at day 50 after tumor induction confirmed the lack of difference between both groups. Mean fluorescence intensities of CD8a, CD68, CD80 and CD206 were not significantly affected by anti-PD-L1 compared to isotype Ctrl treatment in B16F10-GCV mice (Figures 7A,B). In addition, comparable low numbers of macrophages were identified in the LV tissue of anti-PD-L1 and isotype Ctrl treated B16F10-GCV mice, as determined by CD68, CD80 and CD206 fluorescence (Figure 7C). Isotype Ctrl and anti-PD-L1-treated B16F10-GCV animals showed similar degrees of medium to high colocalization for both pro- and anti-inflammatory macrophage markers CD80 and CD206, respectively (Figures 7D–F). Moreover, cardiac CD68, CD206 and CD80 protein expression was not regulated in isotype Ctrl and anti-PD-L1-treated B16F10-GCV mice (Figures 8A–F; Supplementary Figures 8B, 9A–E).

Discussion

In this study, we used a reversible melanoma mouse model (B16F10-GCV) to analyze potential ICI-mediated inflammatory processes in mice, which have been exposed to melanoma disease

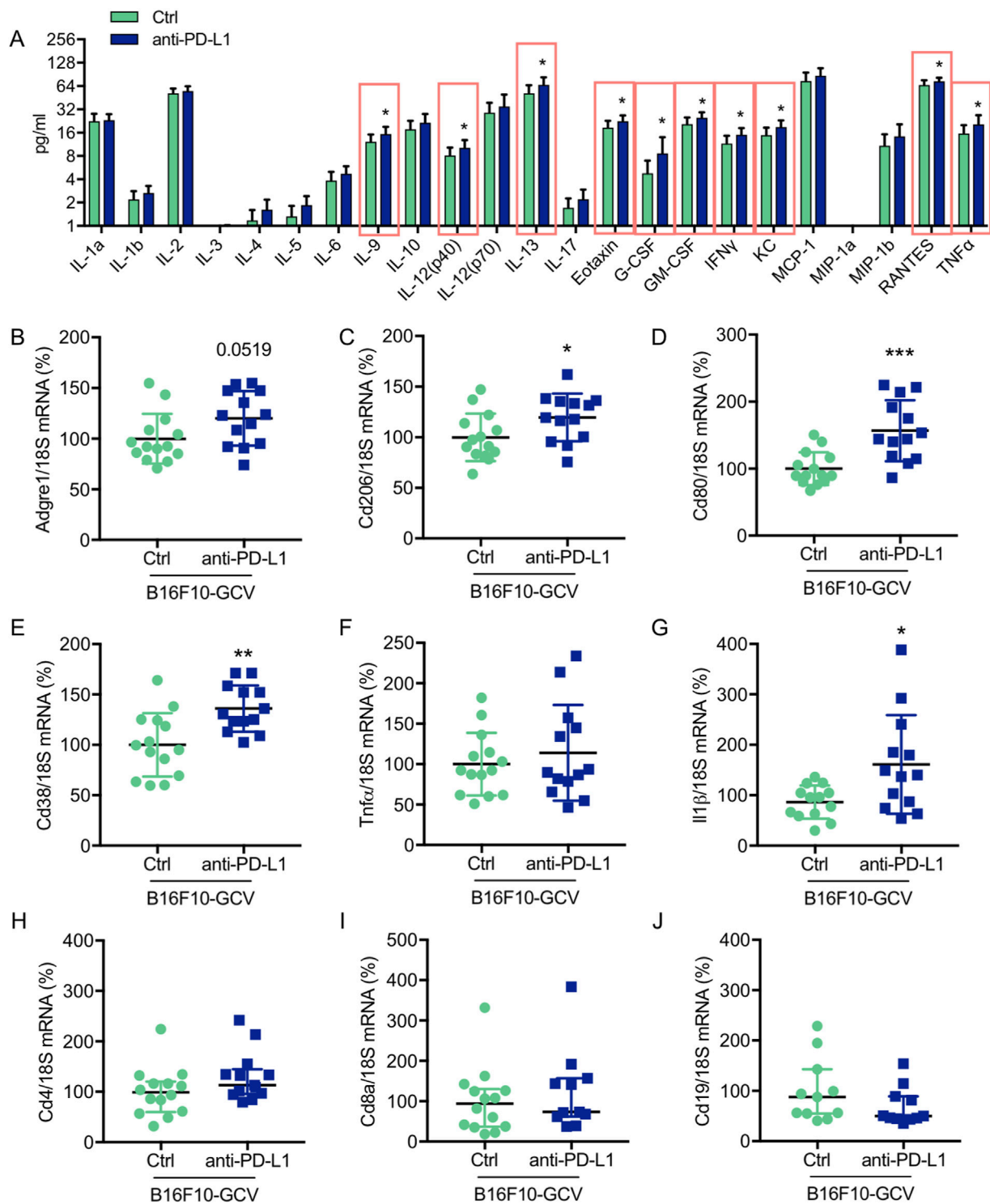


FIGURE 4

Anti-PD-L1 treatment promotes the secretion of inflammatory cytokines/chemokines and the expression of macrophage markers in LV tissue of B16F10-GCV mice (A) Induction of cytokine/chemokine protein concentration in LV tissue lysates of anti-PD-L1 treated B16F10-GCV mice (N = 12) compared to isotype Ctrl treated B16F10-GCV mice (N = 12), measured by Bio-Rad Multiplex Immunoassay System. Dot plots summarizing (B) *Adgre1*, (C) *Cd206*, (D) *Cd80*, (E) *Cd38*, (F) *Tnfr α* , (G) *Il1 β* , (H) *Cd4* and (I) *Cd8a* mRNA levels normalized to 18S RNA analysed by qRT-PCR in B16F10-GCV LVs treated with anti-PD-L1 (N = 13) or isotype Ctrl (N = 14). (J) Dot plot summarizing *Cd19* mRNA levels normalized to 18S RNA analysed by qRT-PCR in B16F10-GCV LVs treated with anti-PD-L1 (N = 11) or isotype Ctrl (N = 11). (B–G) Gaussian distributed data were presented as mean \pm SD and (H–J) not normally distributed data were presented as median and IQR, * $p < 0.05$, ** $p < 0.01$, *** $p < 0.001$ vs. B16F10-GCV isotype Ctrl, unpaired two-tailed Student's *t*-test or Mann-Whitney *U* test.

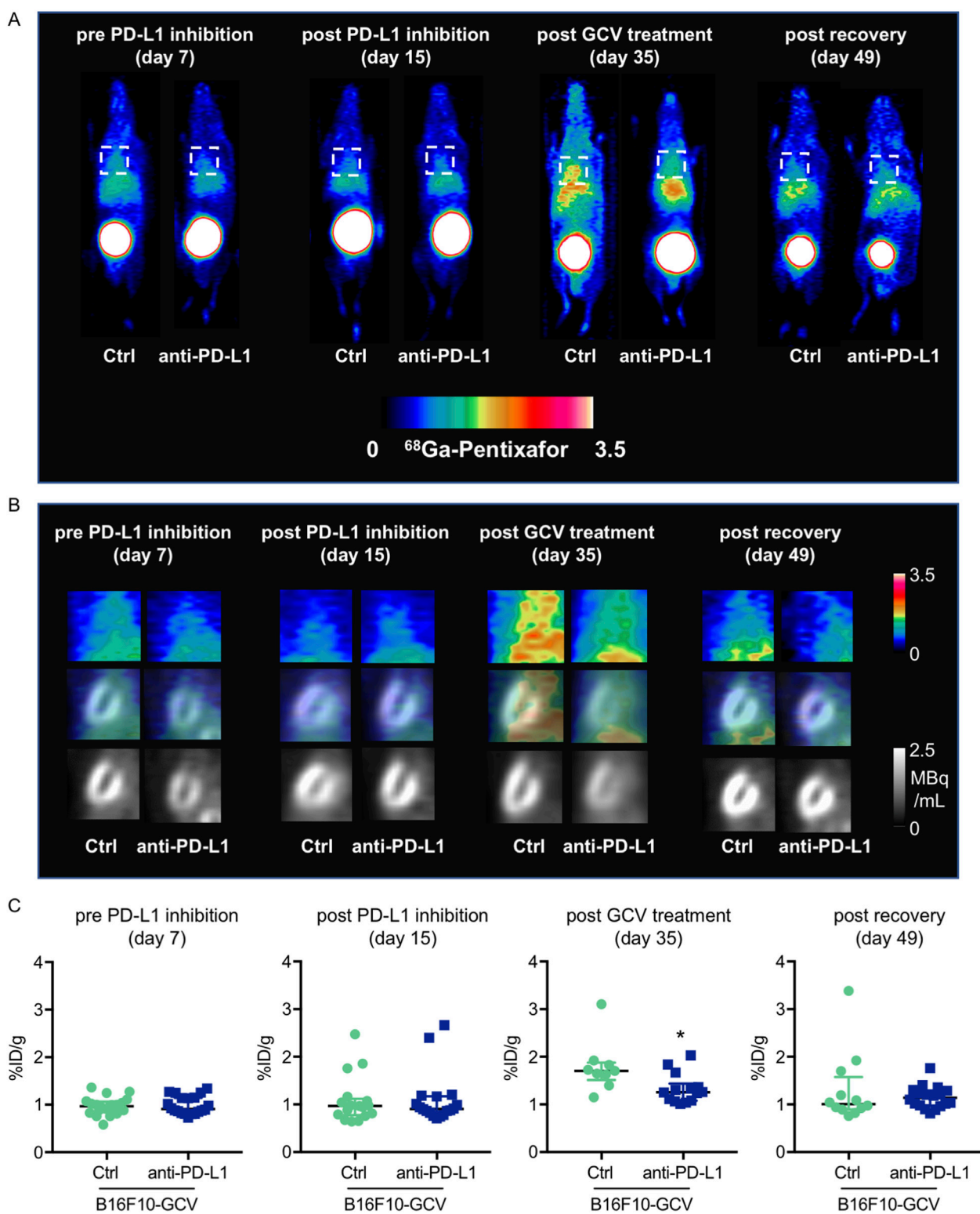


FIGURE 5

Measurements of inflammation by ^{68}Ga -pentixafor in PET-CT of anti-PD-L1 or isotype Ctrl treated B16F10-GCV mice. (A, B) Inflammation was visualized before and after anti-PD-L1 treatment by ^{68}Ga -pentixafor PET-CT and representative (A) whole body and (B) heart images are shown compared to isotype Ctrl B16F10-GCV mice. Regions of interest for data quantification are indicated by squares with dashed lines. (C) Quantitative analysis of percent injected dose per gram tissue in the heart (%ID/g) of ^{68}Ga -pentixafor PET-CT, day 7 anti-PD-L1 (N = 20) vs. isotype Ctrl (N = 20), day 15 anti-PD-L1 (N = 18) vs. isotype Ctrl (N = 17), day 35 anti-PD-L1 (N = 14) vs. isotype Ctrl (N = 9) and day 49 anti-PD-L1 (N = 18) vs. isotype Ctrl (N = 12). Data were presented as median and IQR, statistical analysis was performed using Mann-Whitney *U* test, **p* < 0.05 vs. B16F10-GCV isotype Ctrl.

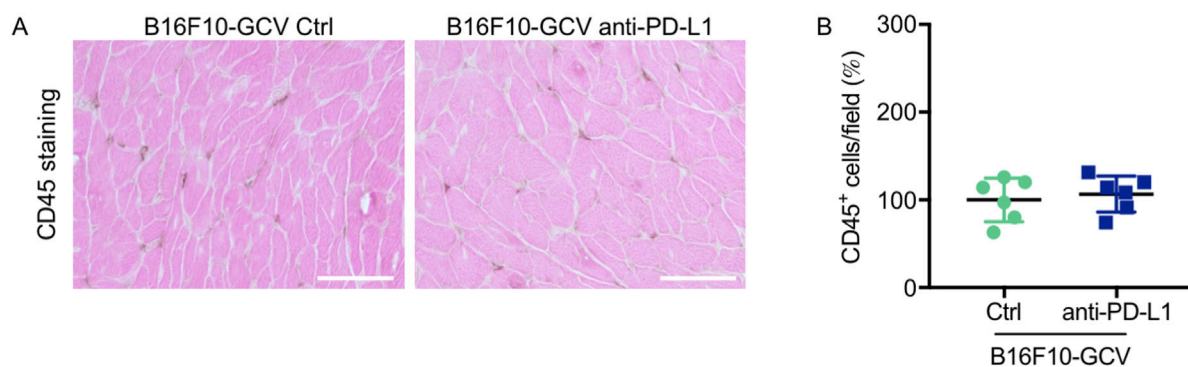


FIGURE 6

Inflammation by CD45 staining of anti-PD-L1 or isotype Ctrl treated B16F10-GCV mice. (A) Staining with the pan-inflammatory marker CD45 (brown, co-stained with eosin) showing inflammation in LV sections from anti-PD-L1-treated B16F10-GCV mice compared to isotype Ctrl-treated B16F10-GCV mice (50 days after tumor induction), scale bars indicate 50 μ m. (B) Dot plot summarizing global inflammation (CD45⁺ cells) calculated as cells/field (in %) in LV sections from anti-PD-L1-treated B16F10-GCV mice (N = 6) compared to isotype Ctrl-treated B16F10-GCV mice (N = 6). Gaussian distributed data were presented as mean \pm SD, n.s. vs. B16F10-GCV isotype Ctrl, unpaired two-tailed Student's t-test.

and are fully recovered without the use of cardiotoxic chemotherapy. In contrast to unchallenged mice, this model might be more representative for ICI administration in cancer patients. The suitability as a model for testing therapy-induced cardiac side effects has already been demonstrated for the known cardiotoxic agent doxorubicin (Pietzsch et al., 2021).

Several studies have suggested that the induction and pathogenesis of autoimmune myocarditis depends on environmental factors and immune-stimulated conditions (Moslehi et al., 2021; Nishimura et al., 2001; Tarrío et al., 2012; Gil-Cruz et al., 2019). For example, a combined knockout of PD-L1/PD-L2 in C57BL/6 mice, which present a rather autoimmune-resistant model, revealed no cardiac phenotype (Keir et al., 2006), whereas Grabie et al. have shown that a transient inflammation of the heart in C57BL/6 mice (Grabie et al., 2007), induced by transgenic cytotoxic T lymphocytes (CTLs) directed against cardiac myocytes, can be transformed to lethal myocarditis by PD-L1 blockade. Also, the deletion of PD-L1 or PD-1 in autoimmune-prone MRL-mice resulted in fatal myocarditis characterized by cardiac infiltration of CD8⁺ and CD4⁺ T cells and macrophages (Lucas et al., 2008; Wang et al., 2010).

Here, we analyzed the potential of PD-L1 inhibition for the development of ICI-induced cardiac inflammation in mice with melanoma cancer disease (B16F10-GCV mice). In our experiments, anti-PD-L1 treatment was associated with an increased survival of B16F10-mice during GCV-mediated tumor elimination, although BLI measurements revealed no difference in tumor burden of surviving anti-PD-L1-treated and control mice (Figures 1B, C). However, differences in size and distribution of tumors at the time of death in the deceased mice cannot be excluded and might have an impact on the survival rate. Indeed, the difference in survival is related to the time frame between 15 and 25 days after tumor induction, a periode after anti-PD-L1 or isotype Ctrl treatment and during the tumor elimination phase with GCV therapy. The effect of PD-L1 blockade on B16F10 tumor growth has been addressed by several reports with different outcomes. While Clark et al.

(2016) and Ji et al. (2021) demonstrated a reduction of B16 tumors in NSG and C57BL/6 mice in response to PD-L1 inhibition, (Choi et al., 2018) and (Pilon-Thomas et al., 2010) showed no effect of anti-PD-L1 monotherapy on the size of B16F10 tumors in C57BL/6 mice. Thus, improved survival of anti-PD-L1-treated mice might represent a systemic effect of PD-L1 inhibition, rather than a direct effect on the tumor.

PD-L1 inhibition itself was not accompanied by cardiotoxic effects in terms of cardiac function and tissue morphology, confirming the observations of the above-mentioned studies, which have shown that blockade of the PD-1/PD-L1 axis itself is not sufficient to induce distinct myocarditis (Keir et al., 2006; Tarrío et al., 2012). In our former studies, we were able to demonstrate that the B16F10-GCV mouse model developed impaired cardiac function in the advanced cancer disease stage, which is reversible after tumor elimination and recovery (Pietzsch et al., 2021). Here, we could confirm the restored cardiac function of the B16F10-GCV model with anti-PD-L1 or isotype Ctrl treatment after recovery from tumor disease (50 days after tumor inoculation). In fact, we observed increased expression of α MHC and TnT, and elevated circulating TNNI3 levels in response to PD-L1 inhibition, but only in B16F10-GCV- and not in GCV-control mice. As mRNA expression of other markers for cardiac pathologic alterations, such as β MHC, and also *Anp*, *Bnp* and *Col1a1* in the LV tissue of B16F10-GCV mice was not affected by PD-L1 inhibition, this rather suggests beneficial remodeling in the heart of mice, which are recovered from tumor disease, than a pathologic effect of PD-L1 inhibition. It cannot be excluded that the combination of anti-PD-L1 treatment and melanoma cancer in the early stages of the disease induced cardiac damage, which was compensated after tumor elimination and recovery and did not result in functional cardiac impairment. Moreover, cardiac ATP2A2 and PLN protein expression and activation was not altered in anti-PD-L1-treated B16F10-GCV mice compared to isotype Ctrl-treated B16F10-GCV mice. The mRNA expression of *Adcy5* and *Adcy6*, which are crucial for β -adrenergic receptor (β -AR) signaling in the heart, is also specifically upregulated by anti-PD-L1 treatment in B16F10-GCV mice, but not in GCV-control mice. While ADCY5 has been reported to be

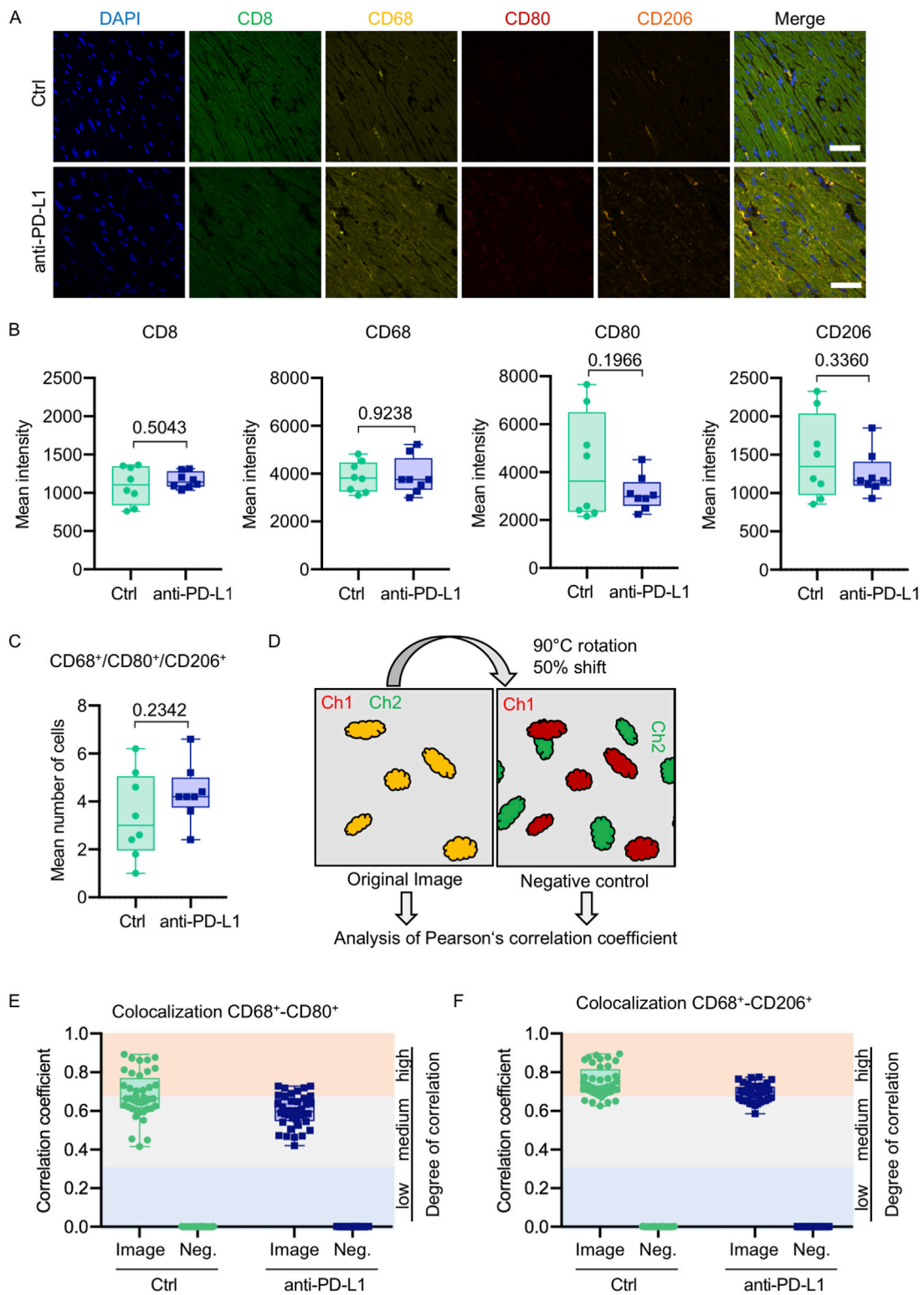


FIGURE 7

Anti-PD-L1 treatment was not associated with an increase of macrophages in the LV of B16F10-GCV mice. (A) Representative immunofluorescence images of immune cell markers in LV sections of anti-PD-L1 or isotype ctrl (Ctrl) treated B16F10-GCV mice. (B) Mean intensities of CD8, CD68, CD80 and CD206 fluorescence signal. One dot represents an average of five regions per animal (N = 8 animals per group). (C) Mean number of macrophages counted in five individual regions within a cardiac section. One dot represents the mean number of macrophages per area per animal (N = 8 animals per group). (D) Scheme of image processing. To generate a negative control image for supervision of random pixel colocalization the second channel (Ch) was rotated and shifted. Both the original image and the negative control image were then analyzed, respectively, for colocalization of fluorescent pixels in both channels. Colocalization analysis between (E) CD68 and CD80 or (F) CD68 and CD206 shown as Pearson's correlation coefficient with respective negative control (Neg.). The colored background indicates the degree of colocalization. Each dot represents the Pearson's correlation

(Continued)

FIGURE 7 (Continued)

coefficient of one field of view in the heart section ($n = 40$, $N = 8$ animals per group). Box plots show median and interquartile range with whiskers from minimum to maximum values. Data were tested for Gaussian distribution and compared using unpaired two-tailed t -test.

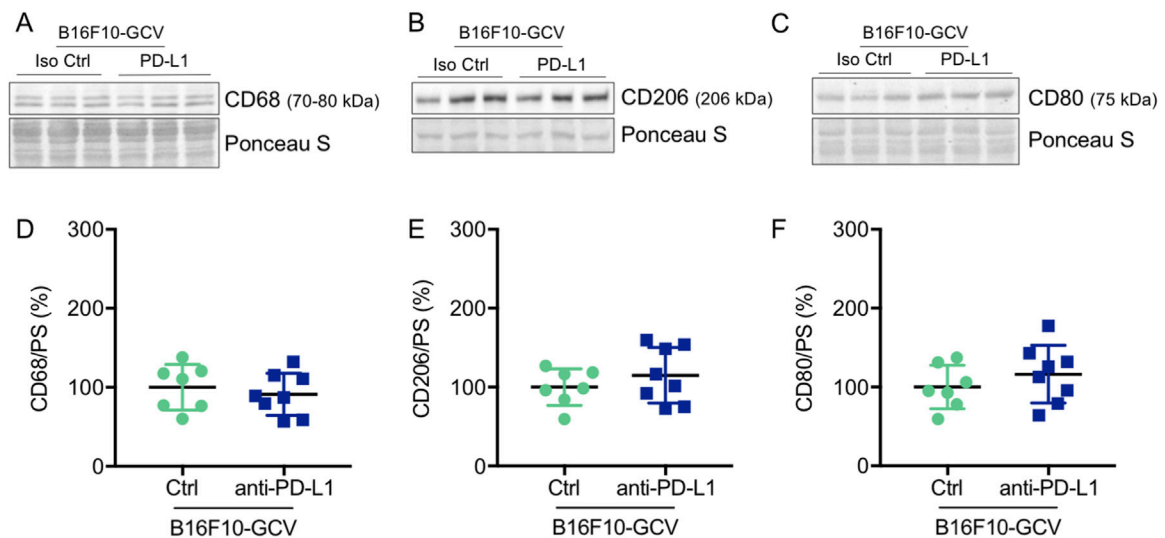


FIGURE 8

Anti-PD-L1 treatment was not associated with an increase in CD68, CD206 and CD80 protein expression in the LV of B16F10-GCV mice. Representative cardiac (A) CD68, (B) CD206 and (C) CD80 western blots and dot plots summarizing quantification of cardiac (D) CD68, (E) CD206 and (F) CD80 protein expression normalized to Ponceau S staining in cardiac tissue of B16F10-GCV LVs treated with anti-PD-L1 ($N = 8$) or isotype Ctrl ($N = 7$). Uncropped full length images are presented in SFig. 9A–E and SFig. 8B. (D–F) Gaussian distributed data were presented as mean \pm SD, n.s vs. B16F10-GCV isotype Ctrl, unpaired two-tailed Student's t -test.

involved in the regulation of oxidative stress (Lai et al., 2013), *Adcy5* upregulation in this study was not associated with transcriptional regulation of *MnSOD* or increased lipid peroxidation as a lipid marker for oxidative stress in B16F10-GCV mice. These data again emphasize that the cardiac phenotype described in this study is specific for PD-L1 inhibition in the context of melanoma disease and that cancer-free mouse models may not be sufficient to analyze ICI-mediated cardiotoxicity.

In contrast, the cardiac mRNA expression of *Ryr2* was increased in anti-PD-L1-treated B16F10-GCV and in GCV mice compared to isotype Ctrl demonstrating that anti PD-L1 *per se* may mediate the expression of several genes involved in the calcium handling independent of melanoma disease.

Numerous studies have demonstrated the induction of T cell-mediated autoimmune myocarditis by the release of cardiac myosin as a result of cardiomyocyte damage (Neu et al., 1987; Smith and Allen, 1991; Neumann et al., 1994; Li et al., 2004; Axelrod et al., 2022). In this study, induction of α MHC mRNA expression in the LV tissue of anti-PD-L1-treated mice was not accompanied by infiltration with T cells or macrophages, as determined by immunohistology.

However, we observed elevated plasma levels of cardiac TNNI3 in response to anti-PD-L1 treatment, indicating the damage of cardiomyocytes. Notably, this was only apparent in B16F10-GCV mice, while in GCV mice PD-L1 inhibition without tumor burden had no effect on α MHC, cardiac TnT and plasma

TNNI3 levels. Furthermore, mRNA levels of the macrophage markers *Cd206*, *Cd38* and *Cd80*, as well as *Il-1 β* , were increased in LV tissue of anti-PD-L1- compared to isotype Ctrl-treated animals, suggesting a mild inflammatory response to PD-L1 inhibition in the heart of B16F10-GCV mice. In GCV control mice, PD-L1 inhibition had no impact on mRNA levels of *Cd206*, *Cd38*, *Cd80* and *Il-1 β* , highlighting the relevance of tumour biology and systemic impact of cancer on the side effects of PD-L1 inhibitors.

Multiplex analysis of cytokine production/secretion in the LV tissue of B16F10-GCV mice confirmed an inflammatory response upon PD-L1 inhibition, which is shaped by cytokines/chemokines that are secreted by several types of immune cells, including macrophages, and are crucial for the promotion of T cell responses. Although an induction of a mild inflammatory response has been demonstrated in anti-PD-L1-treated mice, no accumulation of inflammatory cells was detected in the LV tissue of anti-PD-L1-treated compared to isotype-treated control animals by serial PET-CT/ 68 Ga-Pentixafor measurements or immunohistochemistry. This observation was confirmed by immunohistology data, which did not hint at infiltrating macrophages or T cells in the LV tissue of anti-PD-L1-treated animals, and by Western Blot analysis, which showed comparable protein expression of CD68, CD80 and CD206 in the LV tissue of the animals from both groups. As the cytokine expression profile that was

determined for PD-L1 inhibition is dominated by cytokines and chemokines of an early immune response, with IL-1 and TNF α belonging to the first cytokines released as part of the innate immune response (Bazzoni and Beutler, 1996; Dinarello, 1997), we cannot exclude a later T-cell reaction. PET-CT imaging was performed at time points, covering a period of time (8–42 days following the first ICI application) that represents the median time of onset for ICI-induced myocarditis in clinical studies (30–34 days after starting ICI) (Mahmood et al., 2018; Salem et al., 2018).

Notably, the reported fatality rates were much higher when anti-PD-L1 treatment was combined with anti-CTLA4 treatment compared to anti-PD-L1 monotherapy (Moslehi et al., 2018). Also germline genetic variation of ICI receiving patients is discussed as a potential determinant for occurrence of ICI-induced IRAE (Chin et al., 2022). Therefore, it might be possible that another mouse strain might be more suitable for the display of cardiotoxic effects in this experimental setting.

Surprisingly, in both treatment groups, PET-CT measurements revealed an accumulation of ^{68}Ga -Pentixafor-labeled inflammatory cells following GCV-mediated tumor elimination, which was almost reduced to baseline in recovered animals. This effect was much more pronounced in isotype Ctrl- compared to anti-PD-L1-treated animals and possibly reflects an inflammatory response induced by the tumor or massive GCV-induced lysis of tumor cells (Balkwill and Mantovani, 2001; Mantovani et al., 2008; Vakkila and Lotze, 2004; Lupusoru et al., 2022). Inhibition of PD-L1 might be protective in this context, which is also supported by the reduced mortality of anti-PD-L1-treated B16F10-GCV mice during the tumor elimination phase.

Conclusion

The use of antibody therapies directed against PD-L1 during melanoma cancer disease may mediate longlasting molecular changes in the heart, such as the generation of circulating TNNI3 as a result of moderate cardiac damage and the induction of inflammatory macrophage genes. These alterations did not affect cardiac functions of the animals in our study after tumor elimination and recovery, but may make the heart more susceptible to additional stress over the course of life and thus may partly contribute to late cardiotoxicity. Without a second hit, like an infection that triggers the inflammatory response, anti-PD-L1 treatment appears to be tolerated in the heart in the preclinical melanoma mouse model. Moreover, PD-L1 inhibition in the absence of tumor is unlikely to reflect the systemic immune and physiological response that occurs in combination with cancer, ICI therapy and tumor elimination. Thus, the reversible melanoma mouse model B16F10-GCV provides a useful tool to study cardiac side effects of anti-cancer treatments.

Data availability statement

The raw data supporting the conclusions of this article will be made available by the authors, without undue reservation.

Ethics statement

The animal study was approved by Niedersächsisches Landesamt für Verbraucherschutz und Lebensmittelsicherheit (LAVES), Oldenburg, Germany. The study was conducted in accordance with the local legislation and institutional requirements. All animal studies were in accordance with the German animal welfare legislation and with the European Communities Council Directive 86/609/EEC and 2010/63/EU to protect animals used for experimental purposes under consideration of the ARRIVE guidelines.

Author contributions

CS: Writing–original draft, Writing–review and editing, Conceptualization, Data curation, Formal Analysis, Investigation, Visualization. SP: Conceptualization, Funding acquisition, Investigation, Writing–original draft, Writing–review and editing. CB: Data curation, Formal Analysis, Investigation, Visualization, Writing–review and editing. FM: Data curation, Formal Analysis, Investigation, Visualization, Writing–original draft, Writing–review and editing. FB: Data curation, Formal Analysis, Investigation, Visualization, Writing–review and editing. MK: Data curation, Investigation, Writing–review and editing. AZ: Methodology, Writing–review and editing. SE: Data curation, Formal Analysis, Investigation, Writing–review and editing. CF: Data curation, Formal Analysis, Investigation, Writing–review and editing. EP: Funding acquisition, Methodology, Writing–review and editing. JT: Data curation, Investigation, Visualization, Writing–original draft, Writing–review and editing. DH-K: Conceptualization, Funding acquisition, Writing–review and editing. MR-H: Conceptualization, Data curation, Formal Analysis, Funding acquisition, Investigation, Project administration, Supervision, Validation, Visualization, Writing–original draft, Writing–review and editing.

Funding

The author(s) declare that financial support was received for the research, authorship, and/or publication of this article. This study was supported by the DFG Clinical Research Group KFO311(HI-842/10-2 to DH-K and MR-H; RI-2531/2-2 to MR-H), DFG Grant PO732 to EP, Foundation Leducq (Project ID 19CVD02) to DH-K, Stiftung Gerdes to MR-H and HiLF supported by Life Science Foundation to SP. Funding sources did not have any involvement in the study design, collection, analysis and interpretation of data, writing of the report or the decision to submit the article for publication.

Acknowledgments

The authors wish to thank Birgit Brandt, Jana Keil and Kerstin Beushausen for excellent technical assistance. We thank Renata Stripecke for sharing the HSVtk-construct.

Conflict of interest

The authors declare that the research was conducted in the absence of any commercial or financial relationships that could be construed as a potential conflict of interest.

Publisher's note

All claims expressed in this article are solely those of the authors and do not necessarily represent those of their affiliated

organizations, or those of the publisher, the editors and the reviewers. Any product that may be evaluated in this article, or claim that may be made by its manufacturer, is not guaranteed or endorsed by the publisher.

Supplementary material

The Supplementary Material for this article can be found online at: <https://www.frontiersin.org/articles/10.3389/fmmed.2024.1487526/full#supplementary-material>

References

- Axelrod, M. L., Meijers, W. C., Screever, E. M., Qin, J., Carroll, M. G., Sun, X., et al. (2022). T cells specific for α -myosin drive immunotherapy-related myocarditis. *Nature* 611, 818–826. doi:10.1038/s41586-022-05432-3
- Balkwill, F., and Mantovani, A. (2001). Inflammation and cancer: back to Virchow? *Lancet* 357, 539–545. doi:10.1016/S0140-6736(00)04046-0
- Bazzoni, F., and Beutler, B. (1996). The tumor necrosis factor ligand and receptor families. *N. Engl. J. Med.* 334, 1717–1725. doi:10.1056/NEJM199606273342607
- Chin, I. S., Khan, A., Olsson-Brown, A., Papa, S., Middleton, G., and Palles, C. (2022). Germline genetic variation and predicting immune checkpoint inhibitor induced toxicity. *NPJ Genom Med.* 7, 73. doi:10.1038/s41525-022-00345-6
- Choi, J., Beaino, W., Fecsek, R. J., Fabian, K. P. L., Laymon, C. M., Kurland, B. F., et al. (2018). Combined VLA-4-targeted radionuclide therapy and immunotherapy in a mouse model of melanoma. *J. Nucl. Med.* 59, 1843–1849. doi:10.2967/jnumed.118.209510
- Clark, C. A., Gupta, H. B., Sareddy, G., Pandeswara, S., Lao, S., Yuan, B., et al. (2016). Tumor-intrinsic PD-L1 signals regulate cell growth, pathogenesis, and autophagy in ovarian cancer and melanoma. *Cancer Res.* 76, 6964–6974. doi:10.1158/0008-5472.CAN-16-0258
- De Mello, R. A., Veloso, A. F., Esrom Catarina, P., Nadine, S., and Antoniou, G. (2017). Potential role of immunotherapy in advanced non-small-cell lung cancer. *Oncotargets Ther.* 10, 21–30. doi:10.2147/OTT.S90459
- Dinarelo, C. A. (1997). Interleukin-1. *Cytokine Growth Factor Rev.* 8, 253–265. doi:10.1016/s1359-6101(97)00023-3
- Gil-Cruz, C., Perez-Shibayama, C., De Martin, A., Ronchi, F., Van Der Borgh, K., Niederer, R., et al. (2019). Microbiota-derived peptide mimics drive lethal inflammatory cardiomyopathy. *Science* 366, 881–886. doi:10.1126/science.aav3487
- Glaserapp, A., Derlin, K., Gutberlet, M., Hess, A., Ross, T. L., Wester, H. J., et al. (2021). Molecular imaging of inflammation and fibrosis in pressure overload heart failure. *Circ. Res.* 129, 369–382. doi:10.1161/CIRCRESAHA.120.318539
- Grabie, N., Gotsman, I., Dacosta, R., Pang, H., Stavakis, G., Butte, M. J., et al. (2007). Endothelial programmed death-1 ligand 1 (PD-L1) regulates CD8+ T-cell mediated injury in the heart. *Circulation* 116, 2062–2071. doi:10.1161/CIRCULATIONAHA.107.709360
- Heimerl, M., Sieve, I., Ricke-Hoch, M., Erschow, S., Battmer, K., Scherr, M., et al. (2020). Neuraminidase-1 promotes heart failure after ischemia/reperfusion injury by affecting cardiomyocytes and invading monocytes/macrophages. *Basic Res. Cardiol.* 115, 62. doi:10.1007/s00395-020-00821-z
- Hilfiker-Kleiner, D., Hilfiker, A., Fuchs, M., Kaminski, K., Schaefer, A., Schieffer, B., et al. (2004). Signal transducer and activator of transcription 3 is required for myocardial capillary growth, control of interstitial matrix deposition, and heart protection from ischemic injury. *Circ. Res.* 95, 187–195. doi:10.1161/01.RES.0000134921.50377.61
- Hoch, M., Fischer, P., Stapel, B., Missol-Kolka, E., Sekkali, B., Scherr, M., et al. (2011). Erythropoietin preserves the endothelial differentiation capacity of cardiac progenitor cells and reduces heart failure during anticancer therapies. *Cell. Stem Cell.* 9, 131–143. doi:10.1016/j.stem.2011.07.001
- Ji, S., Lee, J., Lee, E. S., Kim, D. H., and Sin, J. I. (2021). B16 melanoma control by anti-PD-L1 requires CD8+ T cells and NK cells: application of anti-PD-L1 Abs and Trp2 peptide vaccines. *Hum. Vaccin Immunother.* 17, 1910–1922. doi:10.1080/21645515.2020.1866951
- Keir, M. E., Liang, S. C., Guleria, I., Latchman, Y. E., Qipo, A., Albacker, L. A., et al. (2006). Tissue expression of PD-L1 mediates peripheral T cell tolerance. *J. Exp. Med.* 203, 883–895. doi:10.1084/jem.20051776
- Lai, L., Yan, L., Gao, S., Hu, C. L., Ge, H., Davidow, A., et al. (2013). Type 5 adenylyl cyclase increases oxidative stress by transcriptional regulation of manganese superoxide dismutase via the SIRT1/FoxO3a pathway. *Circulation* 127, 1692–1701. doi:10.1161/CIRCULATIONAHA.112.001212
- Li, Y., Heuser, J. S., Kosanke, S. D., Hemric, M., and Cunningham, M. W. (2004). Cryptic epitope identified in rat and human cardiac myosin S2 region induces myocarditis in the Lewis rat. *J. Immunol.* 172, 3225–3234. doi:10.4049/jimmunol.172.5.3225
- Lucas, J. A., Menke, J., Rabacal, W. A., Schoen, F. J., Sharpe, A. H., and Kelley, V. R. (2008). Programmed death ligand 1 regulates a critical checkpoint for autoimmune myocarditis and pneumonitis in MRL mice. *J. Immunol.* 181, 2513–2521. doi:10.4049/jimmunol.181.4.2513
- Lupusoru, G., Ailincăi, I., Fratila, G., Ungureanu, O., Andronesi, A., Lupusoru, M., et al. (2022). Tumor lysis syndrome: an endless challenge in onco-nephrology. *Biomedicines* 10, 1012. doi:10.3390/biomedicines10051012
- Mahmood, S. S., Fradley, M. G., Cohen, J. V., Nohria, A., Reynolds, K. L., Heinzerling, L. M., et al. (2018). Myocarditis in patients treated with immune checkpoint inhibitors. *J. Am. Coll. Cardiol.* 71, 1755–1764. doi:10.1016/j.jacc.2018.02.037
- Mahoney, K. M., Freeman, G. J., and McDermott, D. F. (2015). The next immune-checkpoint inhibitors: PD-1/PD-L1 blockade in melanoma. *Clin. Ther.* 37, 764–782. doi:10.1016/j.clinthera.2015.02.018
- Mantovani, A., Allavena, P., Sica, A., and Balkwill, F. (2008). Cancer-related inflammation. *Nature* 454, 436–444. doi:10.1038/nature07205
- Morton, D. B., and Griffiths, P. H. (1985). Guidelines on the recognition of pain, distress and discomfort in experimental animals and an hypothesis for assessment. *Vet. Rec.* 116, 431–436. doi:10.1136/vr.116.16.431
- Moslehi, J., Lichtman, A. H., Sharpe, A. H., Galluzzi, L., and Kitis, R. N. (2021). Immune checkpoint inhibitor-associated myocarditis: manifestations and mechanisms. *J. Clin. Invest.* 131, e145186. doi:10.1172/JCI145186
- Moslehi, J. J., Salem, J. E., Sosman, J. A., Lebrun-Vignes, B., and Johnson, D. B. (2018). Increased reporting of fatal immune checkpoint inhibitor-associated myocarditis. *Lancet* 391, 933. doi:10.1016/S0140-6736(18)30533-6
- Neilan, T. G., Rothenberg, M. L., Amiri-Kordestani, L., Sullivan, R. J., Steingart, R. M., Gregory, W., et al. (2018). Myocarditis associated with immune checkpoint inhibitors: an expert consensus on data gaps and a call to action. *Oncologist* 23, 874–878. doi:10.1634/theoncologist.2018-0157
- Neu, N., Rose, N. R., Beisel, K. W., Herskowitz, A., Gurri-Glass, G., and Craig, S. W. (1987). Cardiac myosin induces myocarditis in genetically predisposed mice. *J. Immunol.* 139, 3630–3636. doi:10.4049/jimmunol.139.11.3630
- Neumann, D. A., Rose, N. R., Ansari, A. A., and Herskowitz, A. (1994). Induction of multiple heart autoantibodies in mice with coxsackievirus B3- and cardiac myosin-induced autoimmune myocarditis. *J. Immunol.* 152, 343–350. doi:10.4049/jimmunol.152.1.343
- Nishimura, H., Okazaki, T., Tanaka, Y., Nakatani, K., Hara, M., Matsumori, A., et al. (2001). Autoimmune dilated cardiomyopathy in PD-1 receptor-deficient mice. *Science* 291, 319–322. doi:10.1126/science.291.5502.319
- Palaskas, N., Lopez-Mattei, J., Durand, J. B., Iliescu, C., and Deswal, A. (2020). Immune checkpoint inhibitor myocarditis: pathophysiological characteristics, diagnosis, and treatment. *J. Am. Heart Assoc.* 9, e013757. doi:10.1161/JAHA.119.013757
- Pietzsch, S., Wohlan, K., Thackeray, J. T., Heimerl, M., Schuchardt, S., Scherr, M., et al. (2021). Anthracycline-free tumor elimination in mice leads to functional and molecular cardiac recovery from cancer-induced alterations in contrast to long-lasting doxorubicin treatment effects. *Basic Res. Cardiol.* 116, 61. doi:10.1007/s00395-021-00902-7
- Pilon-Thomas, S., Mackay, A., Vohra, N., and Mule, J. J. (2010). Blockade of programmed death ligand 1 enhances the therapeutic efficacy of combination immunotherapy against melanoma. *J. Immunol.* 184, 3442–3449. doi:10.4049/jimmunol.0904114

- Pincha, M., Salguero, G., Wedekind, D., Sundarasetty, B. S., Lin, A., Kasahara, N., et al. (2011). Lentiviral vectors for induction of self-differentiation and conditional ablation of dendritic cells. *Gene Ther.* 18, 750–764. doi:10.1038/gt.2011.15
- Salem, J. E., Manouchehri, A., Moey, M., Lebrun-Vignes, B., Bastarache, L., Pariente, A., et al. (2018). Cardiovascular toxicities associated with immune checkpoint inhibitors: an observational, retrospective, pharmacovigilance study. *Lancet Oncol.* 19, 1579–1589. doi:10.1016/S1470-2045(18)30608-9
- Salloum, F. N., Tocchetti, C. G., Ameri, P., Ardehali, H., Asnani, A., De Boer, R. A., et al. (2023). Priorities in cardio-oncology basic and translational science: GCOS 2023 symposium proceedings: JACC: CardioOncology state-of-the-art review. *JACC CardioOncol* 5, 715–731. doi:10.1016/j.jacc.2023.08.003
- Schardt, J. (2020). The use of immune checkpoint inhibitors in routine oncology. *Z Rheumatol.* 79, 809–817. doi:10.1007/s00393-020-00876-2
- Smith, S. C., and Allen, P. M. (1991). Myosin-induced acute myocarditis is a T cell-mediated disease. *J. Immunol.* 147, 2141–2147. doi:10.4049/jimmunol.147.7.2141
- Tarrio, M. L., Grabie, N., Bu, D. X., Sharpe, A. H., and Lichtman, A. H. (2012). PD-1 protects against inflammation and myocyte damage in T cell-mediated myocarditis. *J. Immunol.* 188, 4876–4884. doi:10.4049/jimmunol.1200389
- Thackeray, J. T., Derlin, T., Haghikia, A., Napp, L. C., Wang, Y., Ross, T. L., et al. (2015). Molecular imaging of the chemokine receptor CXCR4 after acute myocardial infarction. *JACC Cardiovasc Imaging* 8, 1417–1426. doi:10.1016/j.jcmg.2015.09.008
- Thackeray, J. T., Pietzsch, S., Stapel, B., Ricke-Hoch, M., Lee, C. W., Bankstahl, J. P., et al. (2017). Insulin supplementation attenuates cancer-induced cardiomyopathy and slows tumor disease progression. *JCI Insight* 2, e93098. doi:10.1172/jci.insight.93098
- Tomicic, M. T., Thust, R., and Kaina, B. (2002). Ganciclovir-induced apoptosis in HSV-1 thymidine kinase expressing cells: critical role of DNA breaks, Bcl-2 decline and caspase-9 activation. *Oncogene* 21, 2141–2153. doi:10.1038/sj.onc.1205280
- Vakkila, J., and Lotze, M. T. (2004). Inflammation and necrosis promote tumour growth. *Nat. Rev. Immunol.* 4, 641–648. doi:10.1038/nri1415
- Varricchi, G., Galdiero, M. R., Marone, G., Criscuolo, G., Triassi, M., Bonaduce, D., et al. (2017). Cardiotoxicity of immune checkpoint inhibitors. *ESMO Open* 2, e000247. doi:10.1136/esmoopen-2017-000247
- Wang, J., Okazaki, I. M., Yoshida, T., Chikuma, S., Kato, Y., Nakaki, F., et al. (2010). PD-1 deficiency results in the development of fatal myocarditis in MRL mice. *Int. Immunol.* 22, 443–452. doi:10.1093/intimm/dxq026